AIAA JOURNAL
Vol. 50, No. 12, December 2012

High-Speed Rarefied Round Jet and Jet Impingement Flows

Chunpei Cai* and Xionghui Huang†
New Mexico State University, Las Cruces, New Mexico 88003-8001

DOI: 10.2514/1.J051785

This paper presents a gas kinetic study and exact solutions for a few of the problems related to a high-speed collisionless round jet: expanding into vacuum and impinging at a normally set, diffuse, or specular reflective circular plate of finite radius. Several fundamental geometry–velocity relations are used in this study and they play crucial roles. These complete results include flowfield properties and impingement properties at the plate surface. The final results include complex but accurate integrations involving geometry and specific speed ratio factors. Several numerical simulations with the direct simulation Monte Carlo method validate these analytical exact results.

Downloaded by TEXAS A & M UNIVERSITY on March 20, 2013 | http://arc.aiaa.org | DOI: 10.2514/1.J051785

Nomenclature

D	=	nozzle width, m
f	=	Maxwellian velocity distribution function, $\sec^3/\mathrm{m}^3$
k	=	Boltzmann constant, J/K
Kn	=	Knudsen number
K, M, N, J, Q	=	integrand factors of geometry and speed ratio
L	=	distance from nozzle exit to a normally set plate or characteristic length, m
n	=	number density, m^{-3}
P	=	pressure, Pa
p	=	geometry factor
$P_n()$	=	Legendre polynomials
q	=	heat flux at wall, W/m^2
r, θ	=	polar coordinates based on the circular nozzle exit
R	=	universal gas constant, J/(mol K)
R_n	=	nozzle radius, m
R_p	=	plate radius, m
S	=	speed ratio
T	=	temperature, K
U, V, W	=	macroscopic velocity components, m/s
u, v, w	=	molecular velocity components for a zero-velocity-centered Maxwellian distribution, m/s
X, Y, Z	=	point in flowfield, m
y, z	=	one point at circular nozzle exit, m
β	=	$1/(2RT)$, $\sec^2/\mathrm{m}^2$
ϵ	=	temperature ratio T_0/T_w
κ	=	beam index coefficient in cosine law/Simons plume model
λ	=	mean free path, m
W_1, W_2	=	velocity domains
ψ	=	specific zenith angle formed by points $(0,0,0)$, $(X,0,Z)$, and x axis; $=\arctan(Z/X)$
ρ	=	density, kg/m^3
τ	=	shear stress at plate surface, Pa

Subscripts

0	=	for flow properties at circular nozzle exit
1	=	for macroscopic flowfield properties for the problem of free jet expanding into vacuum
2	=	for macroscopic flowfield properties for the problem of jet impingement at a diffuse plate
3	=	for macroscopic flowfield properties for the problem of jet impingement at a specular plate
d	=	for properties related with diffusive reflections
s	=	for properties related with specular reflections
w	=	for properties for wall surface

I. Introduction

A GASEOUS jet expanding into vacuum and a gaseous jet impinging at a normally set plate are fundamental fluid dynamic problems. There are many reports of these problems in the literature. As the counterpart to the continuum flows, highly rarefied jet and jet impingement flows provide a bounding limit and some insights to many problems by solely including molecular movement. In many applications with high Knudsen number or high-speed velocity, the contribution from particle collisions is insignificant. One example of an important application is atomic/molecular beams [1,2], which are a vital tool responsible for many substantial scientific discoveries. Other non-trivial applications include materials processing inside vacuum chambers [3], thermal/chemical/ion/plasma thruster plumes, space weathers [4–6], jet vacuum pumping by diffusion, and ejector pumps [7].

Because there are many applications related to the rarefied jet and jet impingement problems, it is rather difficult to provide a detailed review. Here, we only provide examples for rocket plumes, which are crucial to the rocket and spacecraft community. As the most important signature, rocket plume is a key component for space propulsion, infrared radar detection, and performance evaluations. Because of the importance, many communities have been inves tigating rarefied gaseous jet/plume impingement flows. For example, the bi-annual international rarefied gas dynamics (RGD) sympo siums have been collecting papers on gaseous jet/jet impingement and molecular beams; NASA Johnson Space Center has developed the versatile DSMC Analysis Code (DAC) package with cartesian mesh; one of the major outcomes is to simulate rocket plume impingement [8] at spacecraft surfaces. Kannenberg and Boyd [9] used MONACO code [10] and the cosine law/Simons model [11] to compute the density of a plume impinging at a flat plate. Ivanov and his colleagues developed the SMILE [12] code and performed particle simulations of plume flows from a nozzle. Bartel et al. at Sandia National Laboratory developed the Icarus package with remarkable comprehensive capabilities of chemical/ionization reactions and massively parallel computation [13].

Received 8 December 2011; revision received 19 March 2012; accepted for publication 30 April 2012. Copyright © 2012 by the authors. Published by the American Institute of Aeronautics and Astronautics, Inc., with permission. Copies of this paper may be made for personal or internal use, on condition that the copier pay the $10.00 per-copy fee to the Copyright Clearance Center, Inc., 222 Rosewood Drive, Danvers, MA 01923; include the code 0001-1452/12 and $10.00 in correspondence with the CCC.

*Associate Professor, Department of Mechanical and Aerospace Engineering; ccai@nmsu.edu. Senior Member AIAA.

†Ph.D. Candidate and Research Assistant, Department of Mechanical and Aerospace Engineering.

Downloaded by TEXAS A & M UNIVERSITY on March 20, 2013 | http://arc.aiaa.org | DOI: 10.2514/1.J051785

Compressible gaseous flows usually can be divided into a few regimes according to the Knudsen number (Kn) [14–16]:

$$Kn = \lambda / L \tag{1}$$

where λ is the molecular mean free path and L is a characteristic length. These regimes are 1) continuum ($0 < Kn < 0.01$), 2) velocity slip and temperature jump ($0.01 < Kn < 0.1$), 3) transitional ($0.1 < Kn < 10$), and 4) free molecular or collisionless ($10 < Kn$). For jet and jet impingement at a plate, there are many studies based on continuum theory, such as the Navier–Stokes equations, boundary layer theory, characteristic lines, and Prandtl–Meyer flows [17,18], whereas for the collisionless regime, there are many numerical and experimental studies and reports for the complete flowfield and surface properties. For high-speed gaseous collisionless flows out of an exit, most of the previous studies adopted some simplifications. For example, Noller [19] proposed a solid angle treatment to implicitly consider the nozzle exit geometry. He obtained the plume density field expressed with integrations over solid angles subtended by a flowfield point and the nozzle exit. The cosine law/Simons model [11] treats a rocket plume as exiting from a point source; Narasimha's early investigation [20] indicated that the plume solution is rather complicated, with many cosine functions. Another rocket plume treatment, which is one-dimensional, unsteady, and based on collisionless flows, was suggested by Woronowicz [21]. His treatment splits the exit into many small segments and, as such, the density and pressure distributions in the flowfield can be computed numerically. Furthermore, he proposed the concept of a starting surface, which alleviates the difficulty of this problem. Dettleef provided a comprehensive review on rocket plume and plume impingement flows [22].

This paper presents some recent progress on exact analytical solutions to the problems of collisionless round jet expanding into vacuum and collisionless round jet impingement at a normally set, finite radius circular plate of diffuse or specular reflections. In this paper, a diffuse reflection means that when a particle collides with a flat plate surface, it is reflected at many angles rather than at just one. For a circular plate surface, these angles form a solid angle span of 2π. For a specular reflection case, the reflected particle's normal momentum is reversed, whereas the tangent momentum maintains unchanged. Recently, detailed solutions for high-speed, highly rarefied planar and round plume flows were developed and reported [23–25], followed by some progress on the corresponding plume impingement problems [26]. These solutions only consider collisionless flow situations, such as plasma flows fired from an electric propulsion device. The collision effects are completely omitted and, for the impingement problem, only wall surface properties and diffuse reflections [26] are investigated. Different from other past work, this paper presents gas kinetic analytical studies on the problems of highly rarefied jet and jet impingement flows. It provides detailed, complex, but exact solutions for the collisionless flowfield and surface properties. Because of the complexity of the results, several particle simulations are performed to validate them.

The paper is organized as follows. Section II presents the exact solutions of collisionless, high-speed, gaseous round jets expanding into vacuum; Secs. III and IV present exact solutions to the corresponding problems of high-speed jet impingement at a normally set, finite radius circular flat plate with a diffuse or specular surface; Sec. V includes comparisons of the exact analytical solutions and several direct simulation Monte Carlo (DSMC) [14] simulation results; Sec. VI concludes this paper.

II. Collisionless Free Plume Expanding into Vacuum

The first problem is a collisionless free plume expanding into vacuum from a round nozzle of radius, R_n, with a mean macroscopic velocity of U_0. This section presents the results of number density, velocity, and temperature at a point $P(X, 0, Z)$ in front of the round nozzle. The results are the foundations to study the problems in the next two sections.

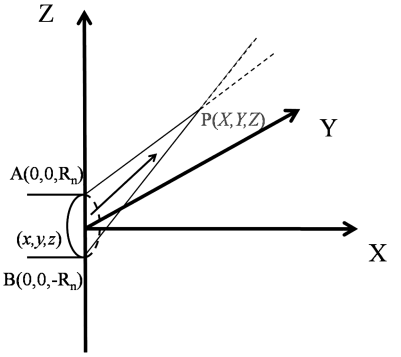

Fig. 1 Illustration of the free plume expansion problem.

Figures 1 and 2 illustrate the problem and the thermal velocity domain for a point $P(X, 0, Z)$. Ω_1 in Fig. 2 is a specific region that relates to the solid angle subtended by the flowfield point $P(X, 0, Z)$ and the circular nozzle exit in Fig. 1. Ω_1 has a conical shape with elliptical cross sections and it extends to $+\infty$.

To generalize the approach for the three problems and to be consistent with the notations in our previous publications [24,25], we use Maxwellian velocity distribution functions at the nozzle exit and the reflective plate. Those molecules leaving the nozzle exit are characterized by the following zero-velocity-centered Maxwellian distribution function:

$$f_0(0, y, z) = n_0(\beta_0/\pi)^{3/2} \exp[-\beta_0(u^2 + v^2 + w^2)] \tag{2}$$

where n_0 is the exit number density and $\beta_0 = 1/(2RT_0)$. To represent the factor of high exit speed U_0, the velocity domain Ω_1 in Fig. 2 shifts from the coordinate origin $(0, 0, 0)$ to point $(-U_0, 0, 0)$. There are parallel relations between these two figures: $PA//P'A'$ and $PB//P'B'$.

Further, from the gas kinetic theory, with a known velocity distribution $f(u, v, w)$ for a flowfield point, the average local number density, velocity components, and temperature can be evaluated using the velocity distribution function [15,16]:

$$n(X, Y, Z) = \iiint_{\Omega} f(u, v, w)\, \mathrm{d}u\, \mathrm{d}v\, \mathrm{d}w \tag{3}$$

$$U(X, Y, Z) = \frac{1}{n(X, Y, Z)} \iiint_{\Omega} u f(u, v, w)\, \mathrm{d}u\, \mathrm{d}v\, \mathrm{d}w \tag{4}$$

$$V(X, Y, Z) = \frac{1}{n(X, Y, Z)} \iiint_{\Omega} v f(u, v, w)\, \mathrm{d}u\, \mathrm{d}v\, \mathrm{d}w \tag{5}$$

$$W(X, Y, Z) = \frac{1}{n(X, Y, Z)} \iiint_{\Omega} w f(u, v, w)\, \mathrm{d}u\, \mathrm{d}v\, \mathrm{d}w \tag{6}$$

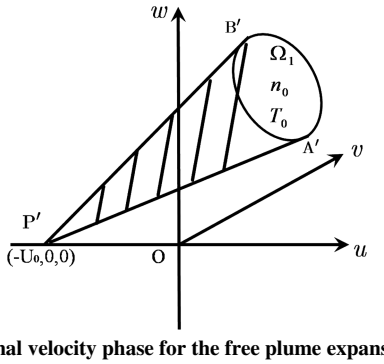

Fig. 2 Thermal velocity phase for the free plume expansion problem.

$$T(X,Y,Z)=\frac{1}{3Rn(X,Y,Z)}\iiint_{\Omega}[(u-U)^2+(v-V)^2+(w-W)^2]f\,\mathrm{d}u\,\mathrm{d}v\,\mathrm{d}w \tag{7}$$

where Ω is the integration domain inside the velocity phase.

The velocity components of those particles escaping from point $(0,y,z)$ at the round nozzle and arriving at point $P(X,Y,Z)$ must satisfy the following constraint, which was revealed recently [25,26]:

$$\frac{X}{u+U_0}=\frac{Y-y}{v}=\frac{Z-z}{w} \tag{8}$$

here, $y=r\cos\theta$ and $z=r\sin\theta$. This relation is an extension from the two-dimensional situation [23], and it plays a crucial role for the approaches and results in this paper. Those particles' velocity components are within W_1 because of the aforementioned relation and the parallel line relations. Equation (8) transforms the solid angle in Fig. 1 into the velocity domain in Fig. 2. Because there are no collisions involved, the velocity domain formed by the right group of molecules at the exit must also be the same one for the flowfield point $P(X,Y,Z)$. The next natural step is to integrate the macroscopic properties according to the gas kinetic formulae. Bearing in mind that the velocity phase for the point $P(X,Y,Z)$ has a conical shape with elliptical cross sections and an infinite length, it is desirable to use a change of variables to transform the infinitely large domain to a finite one. From the constraint condition, the velocity components of the particles in the y and z directions can be written as:

$$v=\frac{-r\cos\theta}{X}(u+U_0);\qquad w=\frac{Z-r\sin\theta}{X}(u+U_0) \tag{9}$$

due to the symmetry of the flowfield, the three-dimensional problem reduces to a problem within the $Y=0$ plane. Equation (9) provides a change of variables:

$$\mathrm{d}\,u\,\mathrm{d}v\,\mathrm{d}w=\frac{(u+U_0)^2}{X^2}r\,\mathrm{d}u\,\mathrm{d}r\,\mathrm{d}\theta$$

The aforementioned relation reduces the integration domain from a semi-infinite one involving u, v, and w to a simpler one related to nozzle exit geometry, r and θ.

Based on the gas kinetic relations, Eqs. (3–7), the final results for the flowfield density, velocity, and temperatures are derived as [25,26]:

$$n_1(X,0,Z)/n_0=\frac{\exp(-S_0^2)}{\sqrt{\pi^3}X^2}\int_{-\pi/2}^{\pi/2}\mathrm{d}\theta\int_0^{R_n}rK\,\mathrm{d}r \tag{10}$$

$$U_1(X,0,Z)\sqrt{\beta_0}=\frac{\exp(-S_0^2)}{\sqrt{\pi^3}X^2}\frac{n_0}{n_1}\int_{-\pi/2}^{\pi/2}\mathrm{d}\theta\int_0^{R_n}rM\,\mathrm{d}r \tag{11}$$

$$W_1(X,0,Z)\sqrt{\beta_0}=\frac{\exp(-S_0^2)}{\sqrt{\pi^3}X^3}\frac{n_0}{n_1}\int_{-\pi/2}^{\pi/2}\mathrm{d}\theta\int_0^{R_n}(Z-r\sin\theta)rM\,\mathrm{d}r \tag{12}$$

$$T_1(X,0,Z)/T_0=-\frac{U_1^2+W_1^2}{3RT_0}+\frac{4}{3}\frac{\exp(-S_0^2)}{\sqrt{\pi^3}X^2}\frac{n_0}{n_1}\int_{-\pi/2}^{\pi/2}\mathrm{d}\theta\int_0^{R_n}Nr\,\mathrm{d}r \tag{13}$$

with the following integrand factors:

$$Q=\cos^2\psi\left[\sum_{n=0}^{\infty}P_n(\sin\psi\sin\theta)\left(\frac{r}{\sqrt{X^2+Z^2}}\right)^n\right]^2 \tag{14}$$

$$K=Q\left[QS_0+\left(\frac{1}{2}+QS_0^2\right)\sqrt{\pi Q}[1+\mathrm{erf}(S_0\sqrt{Q})]\exp(S_0^2Q)\right] \tag{15}$$

$$M=Q^2\left[QS_0^2+1+S_0\left(\frac{3}{2}+QS_0^2\right)\times\sqrt{\pi Q}[1+\mathrm{erf}(S_0\sqrt{Q})]\exp(S_0^2Q)\right] \tag{16}$$

$$N=S_0Q^2\left[\frac{5}{4}+\frac{QS_0^2}{2}\right]+\frac{1}{2}\sqrt{Q^3\pi}\left[\frac{3}{4}+3QS_0^2+Q^2S_0^4\right]\times[1+\mathrm{erf}(S_0\sqrt{Q})]\exp(S_0^2Q) \tag{17}$$

where $P_n(\,)$ are the Legendre polynomials, $\psi=\arctan(Z/X)$, and $S_0=\frac{U_0}{\sqrt{2RT_0}}$. These formulae illustrate that the free plume flowfield solutions contain geometry factors of R, X, and Z, and the velocity factor S_0. As can be seen, the problem of a three-dimensional rarefied free plume expanding from a circular exit has compact solutions.

Along the jet centerline, the expressions for the nondimensional parameters K, M, N, and Q further degenerate. The number density, velocity, and temperature are [27]

$$n_1(X,0,0)/n_0=\frac{1}{2}+\frac{1}{2}\mathrm{erf}(S_0)-\frac{p_1}{2}\exp(-S_0^2p_2^2)[1+\mathrm{erf}(p_1S_0)] \tag{18}$$

$$U_1\sqrt{\beta_0}=\frac{n_0}{2n_1}\left[\frac{p_2^2}{\sqrt{\pi}}\exp(-S_0^2)+S_0[1+\mathrm{erf}(S_0)]-\exp(-p_2^2S_0^2)p_1^3S_0[1+\mathrm{erf}(p_1S_0)]\right] \tag{19}$$

$$T_1(X,0,0)/T_0=-\frac{U_1^2}{3RT_0}+\frac{4}{3}\frac{\exp(-S_0^2)}{\sqrt{\pi}X^2}\frac{n_0}{n_1}\int_0^{R_n}Nr\,\mathrm{d}r \tag{20}$$

where $p_1=X/\sqrt{X^2+R^2}$ and $p_2=R/\sqrt{X^2+R^2}$ are the geometry factors that present in these centerline solutions. The validation work for this problem can be found in one recent paper [27], and the same logic can be extended to compute the flowfield of multiple high-speed jets into vacuum.

III. Collisionless Round Jet Impingement at a Normally Set Diffuse Plate

The problem and the velocity domain pictures for a point $P(X,0,Z)$ between a nozzle of a finite radius R_n and a diffuse reflective plate of a finite radius R_p, which has a distance of L from the nozzle, are illustrated by Figs. 3 and 4. Between these two figures, there are several geometrical relations: $PA//P'A'$, $PB//P'B'$, $PC//OC'$, and $PD//OD'$. The contributions to the flowfield and surface properties are essentially from two different sources, the free plume from the circular nozzle exit and the circular plate surface. They are represented by W_1 and W_2, respectively, in Fig. 4. Both domains extend to infinity.

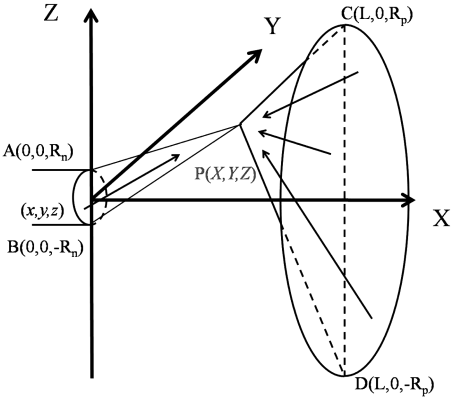

Fig. 3 Illustration of the diffuse reflection impingement problem.

Downloaded by TEXAS A & M UNIVERSITY on March 20, 2013 | http://arc.aiaa.org | DOI: 10.2514/1.J051785

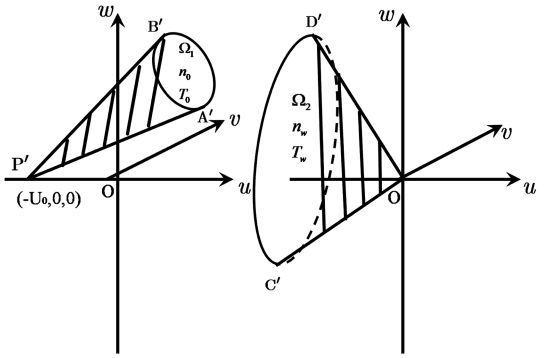

Fig. 4 Thermal velocity phase for the diffuse reflection impingement problem.

Assume the velocity distribution function for those reflected particles from the diffuse surface is

$$f_w(L,0,z) = n_w(L,0,z)(\beta_w/\pi)^{3/2}\exp[-\beta_w(u^2+v^2+w^2)] \tag{21}$$

where $n_w(L,0,z)$ has a distribution over the surface, and it is the only property to be determined by using the condition of zero flux at the plate surface. An integration with u as the moment yields the following relation about n_w:

$$n_1(L,0,z)U_1(L,0,z) = \frac{n_w(L,0,z)}{2\sqrt{\pi\beta_w}} \tag{22}$$

where the subscript "1" represents the free plume flow properties in the flowfield without any plate effects, and the subscript "w" represents the wall, $\beta_w = 1/(2RT_w)$. Equation (22) essentially reveals that based on the fundamental solutions for free plume expanding into vacuum, it is possible to determine the distribution of $n_w(L,0,z)$ for the plate surface.

The computation of the plate effect on the flowfield properties is similar to the free plume situation. The velocity components of the particles that are reflected from a plate point $P_w(L,y,z)$ and arrive at point $(X,0,Z)$ must satisfy the following constraint geometry-velocity condition:

$$\frac{X-L}{u} = \frac{-y}{v} = \frac{Z-z}{w} \tag{23}$$

here, $y = r\cos\theta$ and $z = r\sin\theta$. From this constraint condition, the velocity components of the particles from the plate can be related with geometrical locations:

$$v = \frac{-r\cos\theta}{X-L}u; \qquad w = \frac{Z-r\sin\theta}{X-L}u \tag{24}$$

In the same vein of the approach to solve the problem of a free plume expanding into vacuum and the solutions in Sec. II, the number density, velocity components, and temperature distributions of the flowfield for the second problem are

$$n_2(X,0,Z) = n_1(X,0,Z) + \frac{1}{2\pi X_d^2}\int_{-\pi/2}^{\pi/2}\mathrm{d}\theta\int_0^{R_p} n_w(r,\theta)Q_d^{3/2}r\,\mathrm{d}r \tag{25}$$

$$U_2(X,0,Z)\sqrt{\beta_0} = \frac{e^{-S_0^2}}{X^2\pi^{3/2}}\frac{n_0}{n_2}\int_{-\pi/2}^{\pi/2}\mathrm{d}\theta\int_0^{R_n} Mr\,\mathrm{d}r - \frac{1}{n_2X_d^2\pi^{3/2}\sqrt{\varepsilon}}\int_{-\pi/2}^{\pi/2}\mathrm{d}\theta\int_0^{R_p} n_w(r,\theta)Q_d^2 r\,\mathrm{d}r \tag{26}$$

$$W_2(X,0,Z)\sqrt{\beta_0} = \frac{e^{-S_0^2}}{X^3\pi^{3/2}}\frac{n_0}{n_2}\int_{-\pi/2}^{\pi/2}\mathrm{d}\theta\int_0^{R_n} M(Z-r\sin\theta)r\,\mathrm{d}r + \frac{1}{n_2X_d^3\pi^{3/2}\sqrt{\varepsilon}}\int_{-\pi/2}^{\pi/2}\mathrm{d}\theta\int_0^{R_p}(Z-r\sin\theta)n_w(r,\theta)Q_d^2 r\,\mathrm{d}r \tag{27}$$

$$T_2(X,0,Z)/T_0 = -\frac{U_2^2+W_2^2}{3RT_0} + \frac{4}{3}\frac{e^{-S_0^2}}{X^2\pi^{3/2}}\frac{n_0}{n_2}\int_{-\pi/2}^{\pi/2}\mathrm{d}\theta\int_0^{R_n} Nr\,\mathrm{d}r + \frac{1}{n_2}\frac{1}{2\pi X_d^2\varepsilon}\int_{-\pi/2}^{\pi/2}\mathrm{d}\theta\int_0^{R_p} n_w(r,\theta)Q_d^{3/2}r\,\mathrm{d}r \tag{28}$$

where $\epsilon = T_0/T_w$ is a specific temperature ratio, Q_d is a new geometry parameter that corresponds to Q in Sec. II, except that Q_d uses a factor $X_d = L - X$.

The normalized slip velocity at the plate is as follows:

$$W_2(L,0,Z)\sqrt{\beta_0} = \frac{\exp(-S_0^2)}{X^3\sqrt{\pi^3}}\frac{n_0}{n_2}\int_{-\pi/2}^{\pi/2}\mathrm{d}\theta\int_0^{R_n} M(Z-r\sin\theta)r\,\mathrm{d}r \tag{29}$$

The contribution of the particle velocity distribution at the plate to the slip velocity is zero because the plate is completely diffuse.

As for the plate properties, because the plate normal direction is defined as $(-1,0,0)$ at the plate surface, the pressure, shear stress, and heat flux at the plate have the following formats:

$$T_2(L,0,Z)/T_0 = \frac{n_w}{2n_2(L,0,Z)\varepsilon} + \frac{4\exp(-S_0^2)}{X^2\sqrt{\pi^3}}\frac{n_0}{n_2}\int_{-\pi/2}^{\pi/2}\mathrm{d}\theta\int_0^{R_n} Nr\,\mathrm{d}r \tag{30}$$

$$P_2(L,0,Z) = n_2(L,0,Z)kT_2(L,0,Z) \tag{31}$$

$$C_f = \frac{\tau_{xz}}{\rho_0U_0^2/2} = \frac{4\exp(-S_0^2)}{S_0^2X^3\pi^{3/2}}\int_{-\pi/2}^{\pi/2}\mathrm{d}\theta\int_0^{R_n}(Z-r\sin\theta)QNr\,\mathrm{d}r - \frac{2n_1\beta_0U_1W_2}{n_0S_0^2} + \frac{n_w}{n_0}\frac{\beta_0}{S_0^2\sqrt{\pi\beta_w}}W_2 \tag{32}$$

$$C_q = \frac{q_x}{\rho_0U_0^3/2} = \frac{2\exp(-S_0^2)}{X^2\pi^{3/2}S_0^3}\int_{-\pi/2}^{\pi/2}\mathrm{d}\theta\int_0^{R_n} r\,\mathrm{d}r \times\left[J - 2\frac{Z-r\sin\theta}{X}QNW_2\sqrt{\beta_0}\right] + \frac{n_1\beta_0^{3/2}W_2^2U_1}{n_0S_0^3} - \frac{1}{2}\frac{n_w}{n_0}\frac{1}{\pi^{1/2}S_0^3\varepsilon^{3/2}}(2+\beta_wW_2^2) \tag{33}$$

where

$$J = \frac{Q^2}{2}\left[\left(Q^2S_0^4 + \frac{9}{2}QS_0^2 + 2\right) + \sqrt{\pi Q}S_0 \times\left(Q^2S_0^4 + 5QS_0^2 + \frac{15}{4}\right)\left(1+\mathrm{erf}\left(S_0\sqrt{Q}\right)\right)e^{S_0^2Q}\right] \tag{34}$$

It is possible to obtain the properties along the plume centerline, however, the final results are complex and they are omitted here.

Even though the derivation processes to compute the plate effects are very complex and demanding, the results are accurate. The contribution from the plate to the flowfield can be developed by treating the circular flat plate as a collection of small nozzles with a zero average velocity $S_0 = 0$. This treatment simplifies the integrands Q, M, N, and K.

IV. Collisionless Round Jet Impingement at a Normally Set Specular Wall

The problem and the thermal velocity phase pictures for a flowfield point $P(X,0,Z)$ between a nozzle and a specular plate, which has a distance L from the nozzle, are illustrated by Figs. 5 and 6. An extra "virtual" nozzle is "mirrored" at the other side of the plate. The treatment is very similar to the point source problem in the potential flow theory. Between these two figures, there are several geometrical relations: $PA//P_1'A'$, $PB//P_1'B'$, $PC//P_2'C'$, and $PD//P_2'D'$. The

Downloaded by TEXAS A & M UNIVERSITY on March 20, 2013 | http://arc.aiaa.org | DOI: 10.2514/1.J051785

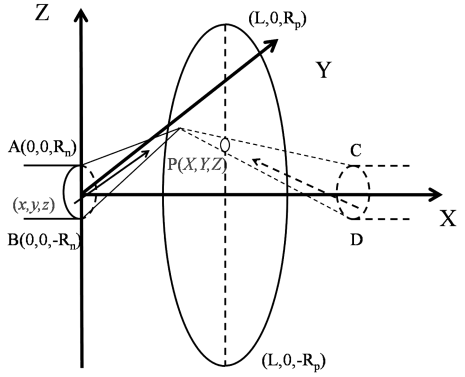

Fig. 5 Illustration of the specular reflection impingement problem.

contributions to the flowfield and surface properties are essentially from two different sources, the free plume from the circular nozzle exit and the circular plate surface. These two sources are represented with W_1 and W_2, respectively, in Fig. 6. There are some differences between a diffuse reflection and a specular reflection scenario because the diffuse case can have particles bounce back along any direction, while the specular plate only bounces each particle along a specific direction. As a result, for the diffuse plate case, an increase of the plate radius R_p increases the plate contribution to the flowfield point $P(X, 0, Z)$, and for a general situation we shall specify a finite plate radius R_p. For a specular reflection scenario, as long as the flowfield point is fully invisible from the virtual nozzle, an increase of plate R_p does not increase the reflected particle contribution to the flowfield point $P(X, 0, Z)$ at all. This difference is illustrated by Figs. 3 and 5. For the specular reflection, the plate contribution to the flowfield point $P(X, 0, Z)$ is from a small patch on the plate, and this contribution can be expressed with the virtual nozzle R_n. To simplify the situation, in this paper we limit our study on the specular plate situation with a condition that $Z < R_p$, such that the flowfield point is always invisible from the virtual nozzle.

To begin the study of this solution, first we need to consider the non-penetration wall boundary condition, the virtual nozzle setup automatically satisfies the specular reflections and the spirit is consistent with the potential flow problem of a point source in front of a wall. The velocity components of the particles that are reflected from the plate and arrive at point $P(X, 0, Z)$ must satisfy the following new velocity-geometry constraint condition:

$$\frac{-X_s}{u - U_0} = \frac{Y - y'}{v} = \frac{Z - z'}{w} \tag{35}$$

here, $X_s = 2L - X$, in which L is the distance from the plate center to the nozzle center; due to the symmetry, we only consider the properties in plane XOZ with $Y = 0$. The variables $y' = r\cos\theta$ and $z' = r\sin\theta$ are located at the virtual nozzle exit. We can rewrite Eq. (35) as

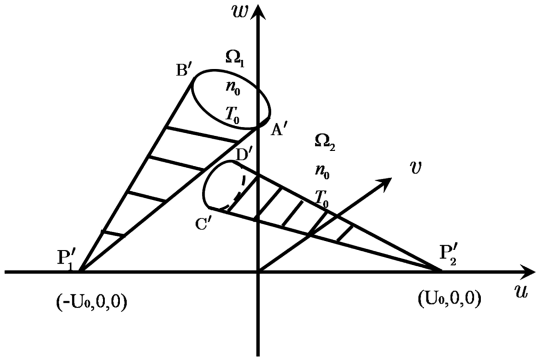

Fig. 6 Thermal velocity phase for the specular reflection impingement problem.

$$v = \frac{-r\cos\theta}{X_s}(u - U_0); \qquad w = \frac{Z - r\sin\theta}{X_s}(u - U_0) \tag{36}$$

The normalized density, velocity components, and temperature at point $P(X, 0, Z)$ are computed as follows:

$$n_3 = \frac{n_0 e^{-S_0^2}}{\pi^{3/2}} \int_{-\pi/2}^{\pi/2} \mathrm{d}\theta \int_0^{R_n} \left(\frac{K}{X^2} + \frac{K_s}{X_s^2}\right) r\,\mathrm{d}r \tag{37}$$

$$U_3(X, 0, Z) = \frac{e^{-S_0^2}}{\pi^{3/2}\sqrt{\beta_0}} \frac{n_0}{n_3} \int_{-\pi/2}^{\pi/2} \mathrm{d}\theta \int_0^{R_n} \left(\frac{M}{X^2} - \frac{M_s}{X_s^2}\right) r\,\mathrm{d}r \tag{38}$$

$$W_3(X, 0, Z) = \frac{e^{-S_0^2}}{\pi^{3/2}\sqrt{\beta_0}} \frac{n_0}{n_3} \int_{-\pi/2}^{\pi/2} \mathrm{d}\theta \int_0^{R_n} \times (Z - r\sin\theta)\left(\frac{M}{X^3} + \frac{M_s}{X_s^3}\right) r\,\mathrm{d}r \tag{39}$$

$$T_3(X, 0, Z)/T_0 = -\frac{1}{3RT_0}(U_3^2 + W_3^2) + \frac{4e^{-S_0^2}}{3\pi^{3/2}} \frac{n_0}{n_3} \int_{-\pi/2}^{\pi/2} \mathrm{d}\theta \int_0^{R_n} \left(\frac{N}{X^2} + \frac{N_s}{X_s^2}\right) r\,\mathrm{d}r \tag{40}$$

where

$$Q_s = \cos^2\psi' \left[\sum_{n=0}^{\infty} P_n\left(\sin\psi'\sin\theta\right)\left(\frac{r}{\sqrt{X_s^2 + Z^2}}\right)^n\right]^2 \tag{41}$$

and ψ' is a geometry angle formed by the point, $P(X, 0, Z)$, the X-axis, and the "virtual" nozzle center. This angle corresponds to the ψ angle in Sec. II.

$$K_s = Q_s^2 S_0 + \left(Q_s^2 S_0^2 + \frac{Q_s}{2}\right)\sqrt{\pi Q_s}\left(1 + \mathrm{erf}\left(S_0\sqrt{Q_s}\right)\right) e^{S_0^2 Q_s} \tag{42}$$

$$M_s = Q_s^2\left[Q_s S_0^2 + 1 + S_0\left(Q_s S_0^2 + \frac{3}{2}\right) \times \sqrt{\pi Q_s}\left[1 + \mathrm{erf}\left(S_0\sqrt{Q_s}\right)\right] e^{S_0^2 Q_s}\right] \tag{43}$$

$$N_s = \frac{Q_s}{2}\left[Q_s S_0\left(Q_s S_0^2 + \frac{5}{2}\right) + \sqrt{\pi Q_s}\left(Q_s^2 S_0^4 + 3Q_s S_0^2 + \frac{3}{4}\right) \times \left(1 + \mathrm{erf}\left(S_0\sqrt{Q_s}\right)\right) e^{S_0^2 Q_s}\right] \tag{44}$$

Along the X-axis, Q_s, K_s, M_s, and N_s degenerate. The number density, velocity, and temperature are

$$n_3(X, 0, 0)/n_0 = 1 + \mathrm{erf}(S_0) - \frac{p_1}{2}\exp(-S_0^2 p_2^2)[1 + \mathrm{erf}(p_1 S_0)] - \frac{p_3}{2}\exp(-S_0^2 p_4^2)[1 + \mathrm{erf}(p_2 S_0)] \tag{45}$$

$$U_3(X, 0, 0)\sqrt{\beta_0} = \frac{n_0}{2n_3}\left[\frac{p_2^2 - p_4^2}{\sqrt{\pi}}\exp(-S_0^2) - \exp(-p_2^2 S_0^2) p_1^3 S_0 \times [1 + \mathrm{erf}(p_1 S_0)] + \exp(-p_4^2 S_0^2) p_3^3 S_0 [1 + \mathrm{erf}(p_3 S_0)]\right] \tag{46}$$

$$T_3(X, 0, 0)/T_0 = -\frac{U_3^2}{3RT_0} + \frac{4e^{-S_0^2}}{3\pi^{1/2}} \frac{n_0}{n_3} \int_0^{R_n} \left(\frac{N}{X^2} + \frac{N_s}{X_s^2}\right) r\,\mathrm{d}r \tag{47}$$

where $p_3 = X_s/\sqrt{X_s^2 + R^2}$ and $p_4 = R_n/\sqrt{X_s^2 + R^2}$ are geometric factors presented in these centerline solutions.

Considering that the normal surface pressure at a plate is the component along the normal direction only, the pressure coefficient along the specular reflection wall is as follows:

Downloaded by TEXAS A & M UNIVERSITY on March 20, 2013 | http://arc.aiaa.org | DOI: 10.2514/1.J051785

$$C_p = \frac{1}{2S_0^2}\left[-\frac{n_3}{n_0}\frac{W_3^2}{3RT_0} + \frac{8e^{-S_0^2}}{3X^2\pi^{3/2}}\int_{-\pi/2}^{\pi/2} \mathrm{d}\theta \int_0^{R_n} Nr\,\mathrm{d}r\right] \quad (48)$$

Because of the symmetry in this problem, the shear stress and heat flux at the plate surface are zero.

V. Validations

This section includes numerical validations using the DSMC method. For these simulations, it is assumed that the test gas is argon and the nozzle diameter $D = 0.2$ m. All simulations are performed with a special DSMC package, GRASP, with the $-P$ module [28]. This module is a general purpose particle simulation package with special object-oriented programming styles and software engineering design patterns. In the DSMC simulations for the free plume problem, an inlet boundary represents the nozzle exit at the lower left corner, a symmetric line for the plume centerline, and vacuum boundaries for other sides. For the plume impingement problems, a vertical line segment is adopted to represent the diffuse or specular circular plate, which locates at the right side of the simulation domain. The plate length R_p and the nozzle-plate center-to-center distance L are both set to 10 times the nozzle radius R_n. For the DSMC simulations in this paper, the Knudsen number is set to $Kn = 100$ and the analytical results are truly collisionless. The simulation package is dimensional and requires specifications of number density at the left nozzle exit. If the $Kn = 100$ simulation results agree well with the analytical collisionless results, we expect higher Kn numbers or collisionless simulation results to have even better agreement with the analytical results.

Most of the aforementioned analytical solutions involve several integral terms that cannot be analytically evaluated, and these numerical evaluations are performed by quadrature.

A. Rarefied Free Jet Expanding into Vacuum

For the scenario of free collisionless plume flow expanding into vacuum, we only present some flowfield results of n, u, v, and p to validate the solutions. This is based on two considerations. First, one recent paper [27] reported a comprehensive validation of all Kn number ranges for a free plume expanding into vacuum by comparing it with the cosine law/Simons plume model. Second, the jet impingement flow solutions are based on these free plume solutions. If the impingement solutions are validated, they provide strong support for the free plume solutions.

Before the validation results are presented, the cosine law/Simons model has to be briefly reviewed. The cosine law/Simons plume model [11] has been widely adopted for at least half a century. If the mass flow in the boundary were actually inviscid, it would expand and distribute itself in the plume according to the cosine law. Using the continuity equation, the density at any point in the plume can be computed in a closed form based on the condition in the nozzle with the following equation:

$$\frac{\rho}{\rho_s} = \frac{n}{n_s} = A\left(\frac{R_0}{r}\right)^2 f(\theta) \quad (49)$$

where R_0 is the orifice radius and A is a constant obtained from the continuity of the rocket-mass flow. It is a function of the specific heat ratio and the exit Mach number, and $f(\theta)$ is a plume angular density decay function. The function $f(\theta)$ is best duplicated by a cosine power function [11]:

$$f(\theta) = \cos^{\kappa}\left(\frac{\pi}{2}\frac{\theta}{\theta_{\max}}\right) \quad (50)$$

where $\theta_{\max}$ is an angular scale and κ is a constant determined by the gas specific heat ratio, which accounts for observed deviation at a non-zero average velocity of the plume.

Figure 7 presents normalized number density contours. The nozzle lip point is actually a singularity point for the density field with large gradients. It is evident that the analytical and DSMC results are essentially identical and the cosine law model relative departure.

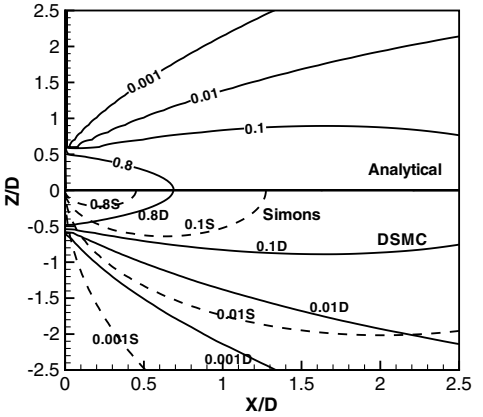

Fig. 7 Free plume: normalized number density, $S_0 = 2.0$. Solid lines: DSMC (bottom), analytical (top); dashed lines: Simons (bottom).

Figures 8 and 9 show the normalized U- and V-velocity component contours. Along the flow direction, faster molecules have higher chances to be observed; as such, the U-velocity component increases. Along the vertical direction, molecules' velocity increases from zero because of the symmetric condition at the jet centerline. Figure 10 shows the analytical and DSMC results of the normalized pressure contours at high Kn numbers, and the result is consistent with the density contours. In general, the analytical and DSMC contours are essentially identical. One recent paper [27] includes more detailed numerical comparisons of the new collisionless flow solutions, and the DSMC simulation results of rarefied jet flows.

Before the end of this subsection, several discussions are offered as follows:

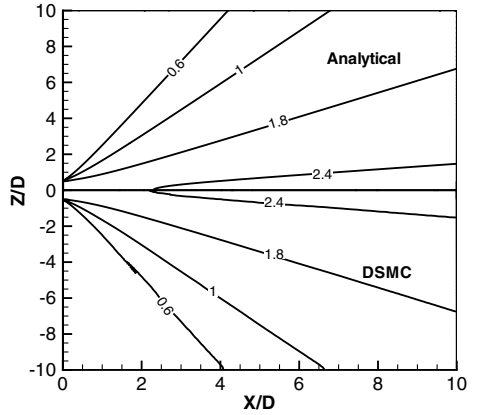

Fig. 8 Free plume: normalized U-velocity contours, $S_0 = 2.0$, analytical (top) and DSMC (bottom).

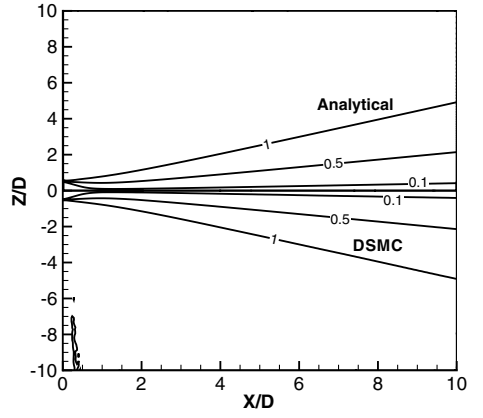

Fig. 9 Free plume: normalized V-velocity contours, $S_0 = 2.0$.

Downloaded by TEXAS A & M UNIVERSITY on March 20, 2013 | http://arc.aiaa.org | DOI: 10.2514/1.J051785

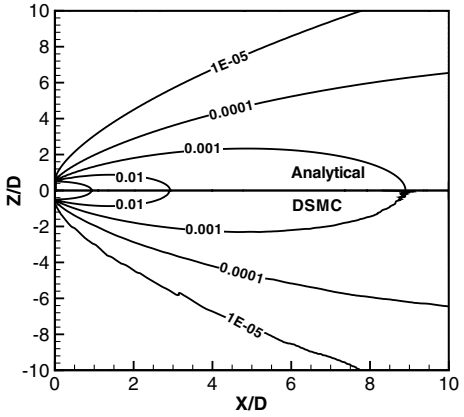

Fig. 10 Free plume: normalized pressure contours, $S_0 = 2.0$.

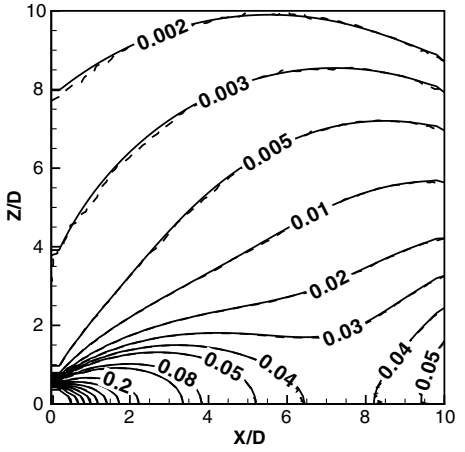

Fig. 11 Diffuse reflection: simulation and analytical results of normalized number density, $S_0 = 2.0$, $\epsilon = 1$.

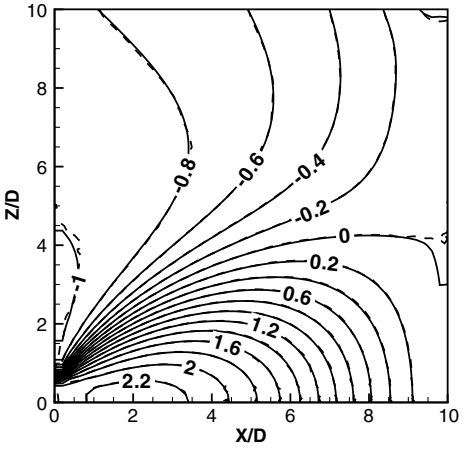

Fig. 12 Diffuse reflection: simulation and analytical results of normalized U-velocity component, $S_0 = 2.0$, $\epsilon = 1$.

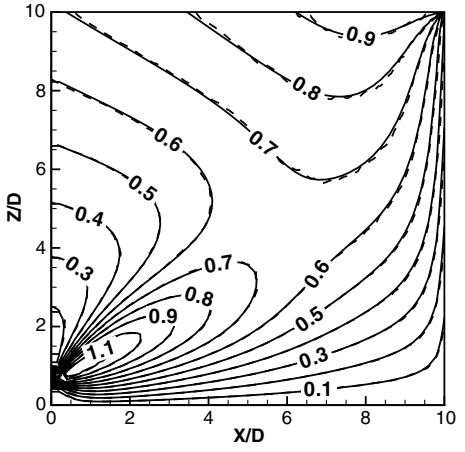

Fig. 13 Diffuse reflection: simulation and analytical results of normalized W-velocity component, $S_0 = 2.0$, $\epsilon = 1$.

Downloaded by TEXAS A & M UNIVERSITY on March 20, 2013 | http://arc.aiaa.org | DOI: 10.2514/1.J051785

1) Even though the set of formulae are derived for collisionless flows, they are applicable for transitional and near continuum flow regimes as well if at the exit the gas speed is high [27]. This is due to the physical fact that if gas flows in a fast downstream direction, there is no time for the molecules to diffuse vertically. As such, high-speed near-continuum plume flows can be well approximated by collisionless jet flows.

2) Similar to most past models reported in the literature, either continuum or free molecular, the cosine law/Simons model does not consider the jet exit speed ratio S_0 explicitly; θ is a pure geometrical factor. However, this set of gas kinetic free plume solutions, Eqs. (10–13), include both the geometrical factors Q, K, M, and N and the speed ratio S_0.

3) The new gas kinetic solutions provide complete and accurate flowfields of density, velocity, and pressure with several complex factors of the speed ratio S_0 and geometrical factors; by comparison, the widely used cosine law/Simons model provides a density field only with a simple cosine function with beam factors.

4) Even for density, the new gas kinetic solutions are more accurate than the Simons model because the former contains more geometrical factors. In the same vein, Chen [29] reported some numerical results of drag force for plasma plume impingement at an inclined flat plate.

5) The cosine law/Simons model may seem concise; however, the same need of a computer reduces its advantage over the new gas kinetic solutions.

6) This set of gas kinetic solutions is valid not only for a free jet into a vacuum, it is also a foundation to solve for jet impingement at a plate. Further, the solutions can be extended to the situations of multiple or a cluster of free jets into vacuum. Applications include a cluster of electric propulsion thrusters in space propulsion and materials processing inside a vacuum chamber with multiple nozzles for different materials.

For the whole flowfield, the gas kinetic model solutions are relatively more complete and more accurate, with a wider range of applications for gas flows from the collisionless regime to near continuum regime. As such, they can supercede or replace the cosine law/Simons plume model.

It shall be emphasized that all of these are due to the crucial geometry-velocity relation, i.e., Eq. (8).

B. Jet Impingement at a Diffuse Reflective Flat Plate

Figure 11 compares analytical collisionless flow density results, Eq. (25), and the corresponding results from DSMC simulations. Because of the plate blockage, particles accumulate in front of the plate and density increases. Figures 12 and 13 compare the corresponding velocity components; due to the non-penetration condition, the plate surface is a zero U-velocity line. Also, because of the diffuse reflections, the slip velocity along the surface is also zero. For the whole flowfield, the v-velocity component is larger than zero, which means that molecules are leaving the central region. Figures 14 and 15 compare temperature and pressure fields, respectively. Even though the flows are collisionless, we observed a temperature increase in front of the plate. The speed ratio was set to 2.0 for the DSMC simulations.

These figures yield the following conclusions:

1) The analytical and numerical simulation results are sufficiently close. This fact indicates that the approach and the analytical and DSMC simulation results are valid for this diffuse reflection case.

2) There is no observation of $\partial(\,)/\partial x = 0$ patterns at the flat diffuse plate surface.

3) The U-velocity at the plate is zero to satisfy the zero flux wall boundary condition.

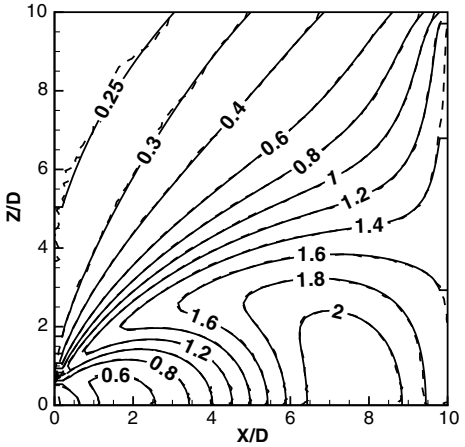

Fig. 14 Diffuse reflection: simulation and analytical results of normalized temperature, $S_0 = 2.0$, $\epsilon = 1$.

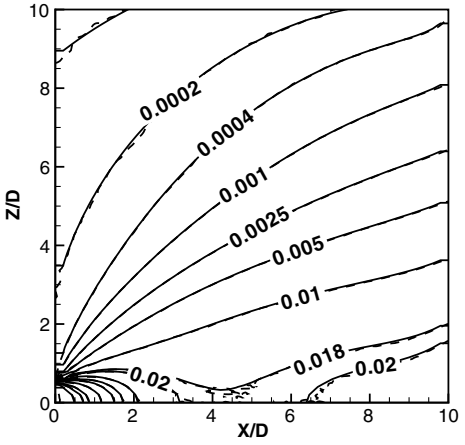

Fig. 15 Diffuse reflection: simulation and analytical results of normalized flowfield pressure, $S_0 = 2.0$, $\epsilon = 1$.

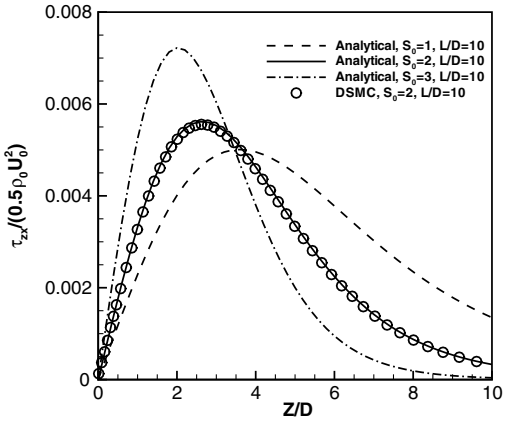

Fig. 17 Diffuse reflection: simulation and analytical results of wall shear stress, $\epsilon = 1$.

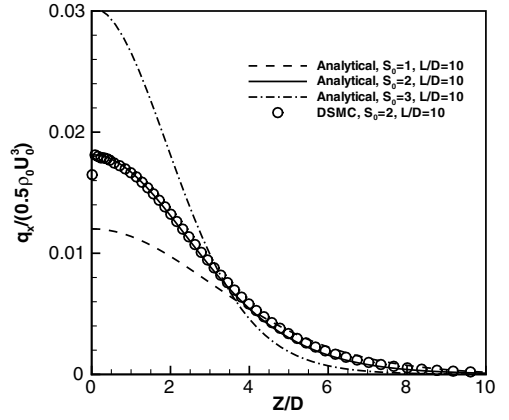

Fig. 18 Diffuse reflection: simulation and analytical results of wall heat flux, $\epsilon = 1$.

Downloaded by TEXAS A & M UNIVERSITY on March 20, 2013 | http://arc.aiaa.org | DOI: 10.2514/1.J051785

4) At regions close to the plate, the pressure distribution has high values.

5) The temperature distribution at the wall is relatively low due to the cold wall temperature boundary conditions.

Figures 16–18 show the normalized surface distributions of pressure, shear stress, and heat flux coefficients. They illustrate that the speed ratio effects on these coefficients, and several exact curves of different S_0 are included. When the gas is collisionless, an increase of the speed ratio results in steeper and narrower plate surface pressure and heat flux profiles because incoming particles have higher kinetic energy and less time to depart normally from the jet flow direction. However, for the shear stress distributions, there is no monatomic changes for the maximum stress value and location.

It shall be emphasized for this problem, geometry-velocity relations are also crucial.

C. Jet Impingement at a Specular Reflective Flat Plate

Figure 19 compares analytical collisionless flow density results, Eq. (37), and the corresponding results from DSMC simulations. In general, the agreement is satisfying. Figures 20 and 21 compare the corresponding velocity components. In the core region, the

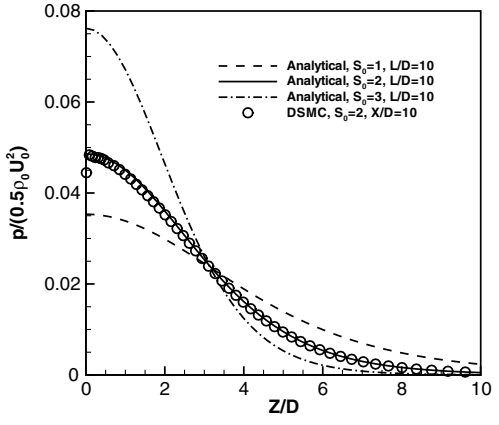

Fig. 16 Diffuse reflection: C_p distribution along the wall surface, $\epsilon = 1$.

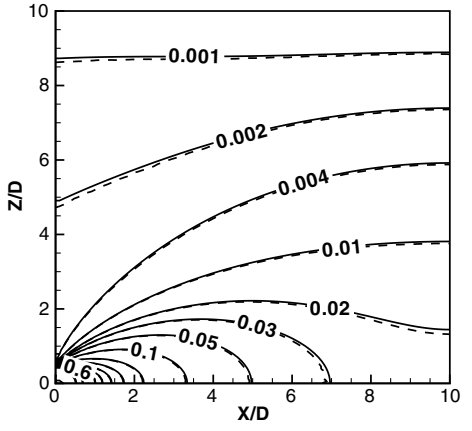

Fig. 19 Specular reflection: simulation and analytical results of normalized flowfield number density, $S_0 = 2.0$.

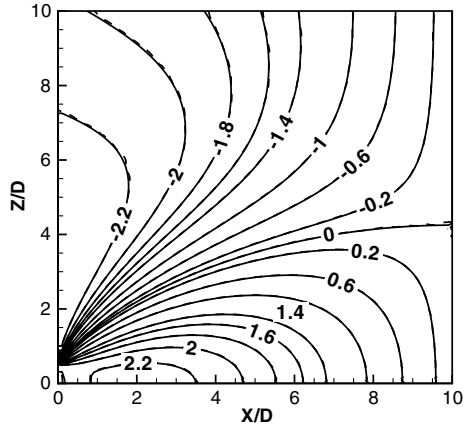

Fig. 20 Specular reflection: simulation and analytical results of normalized flowfield U-velocity component, $S_0 = 2.0$.

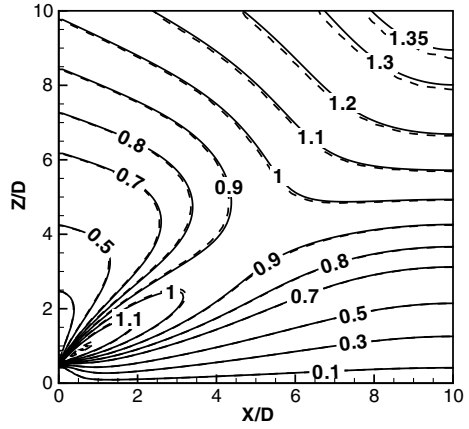

Fig. 21 Specular reflection: simulation and analytical results of normalized flowfield W-velocity component, $S_0 = 2.0$.

U-velocity component is positive because the real nozzle effect dominates over that virtual nozzle. Above the real nozzle, the values are negative, indicating weaker contribution from the real nozzle. The V-velocity component figure has no negative values, which can be easily understood by the contributions from the two nozzles, in which all molecules flow out from the jet central region. Figures 22 and 23 compare the exact analytical and DSMC simulation results of the temperature and pressure fields. In these four figures, the specific exit speed ration is $S_0 = 2$. These four figures lead to the following conclusions:

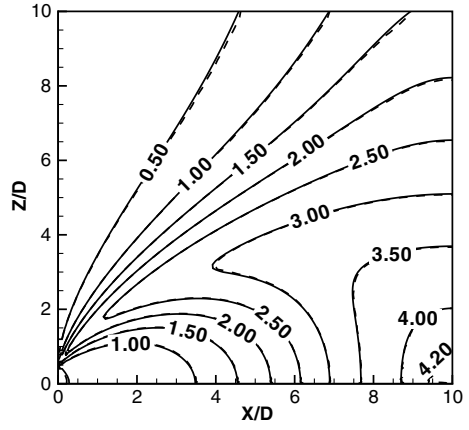

Fig. 22 Specular reflection: simulation and analytical results of normalized flowfield temperature, $S_0 = 2.0$.

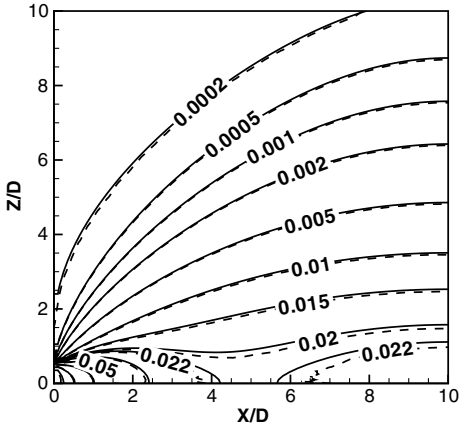

Fig. 23 Specular reflection: simulation and analytical results of normalized flowfield pressure, $S_0 = 2.0$.

1) The analytical and numerical simulation results are also sufficiently close, which indicates the approach and results are correct for this specular reflection case.

2) Because the plate surface is specular, to satisfy the nonpenetration boundary conditions, an equal strength "virtual" nozzle is mirrored at the other side of the plate. As a direct result, all the flow patterns are symmetric about the plate, with $\partial(\,)/\partial n = 0$ at the plate surface.

3) The U-velocity at the plate is zero to satisfy the zero-flux wall boundary condition.

4) At regions close to the plate, the temperature is higher than the diffuse reflection case. At this region, there are two groups of molecules moving along opposite directions but with exactly opposite speeds. As a result, the velocity distribution function has a much wider span there, which means a higher temperature.

Figure 24 shows several pressure coefficient distributions along a specular reflective surface. It compares the speed ratio effects on surface pressure and several exact curves with different S_0 are included. If the gas is collisionless, then an increase of the speed ratio results in steeper and narrower pressure profiles because incoming particles have high velocity and less time to depart normally from the jet flow direction. Compared with the counterpart in the diffuse plate scenario, Fig. 24 shows relatively lower values; whether this is a general fact still needs to be investigated. Because of the symmetry, the heat flux and shear stress is zero along the wall surface.

Figure 25 shows profiles of centerline density for jet impingement at a specular reflective flat plate with several different speed ratios. As the speed ratio increases, more molecules flow from the nozzle and this results in higher density profiles. The $S_0 = 2$ profile is validated by DSMC simulations. Figure 26 shows profiles of centerline

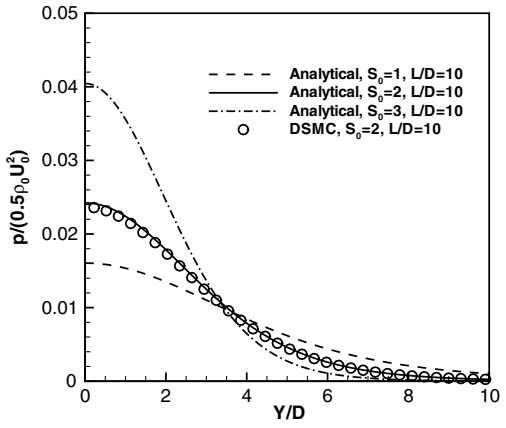

Fig. 24 Specular reflection: normalized pressure distribution along plate surface.

Downloaded by TEXAS A & M UNIVERSITY on March 20, 2013 | http://arc.aiaa.org | DOI: 10.2514/1.J051785

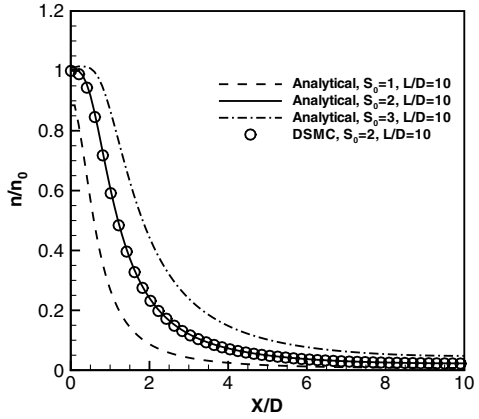

Fig. 25 Specular reflection: normalized number density profiles along the jet centerline.

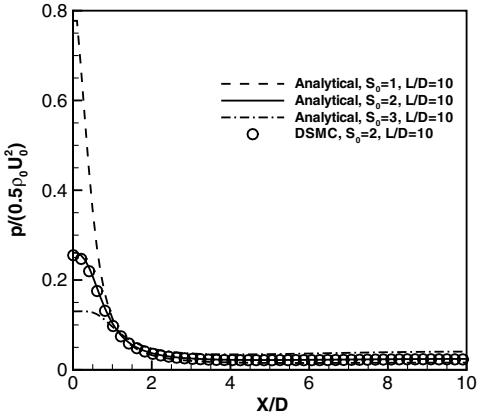

Fig. 26 Specular reflection: normalized pressure profiles along the jet centerline.

pressure, collisionless flows with different S_0 values. The higher pressure distribution of larger S_0 is consistent with the higher number density profiles in Fig. 25. Figure 27 shows profiles of centerline temperature for the case of a specular reflective flat plate with different S_0. The temperature close to the plate is much higher than the scenario of a diffuse plate. Figure 28 illustrates the speed ratio S_0 effects on the centerline velocity; as the ratio increases, the velocity profiles shift up, meaning higher molecular kinetic energy. All curves converge to zero at the plate surface to satisfy the zero-flux condition. It shall be pointed out that the last two pictures have non-monatomic trends, and this indicates the competing effects between the real and virtual nozzles.

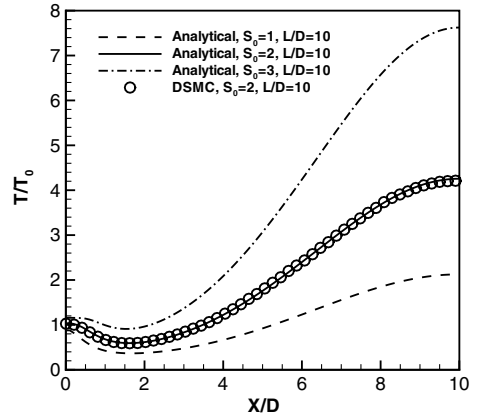

Fig. 27 Specular reflection: normalized temperature profiles along the jet centerline.

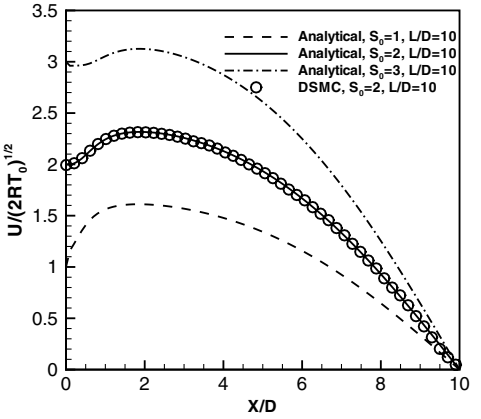

Fig. 28 Specular reflection: normalized *U*-velocity profiles along the jet centerline.

VI. Conclusions

In conclusion, this paper presents fundamental gas kinetic studies of collisionless flows from a circular exit: free round jet expanding into vacuum, free jet impingement at a normally set diffuse, or a specular reflective circular flat plate with a finite radius. The fundamental assumptions are the Maxwellian distributions at the nozzle exit, the plate surface, and the virtual nozzle. Crucial geometry-velocity relations are adopted to change integration variables, and complex but accurate formulae are obtained. Flowfield property formulae, which include number density, velocity, temperature, and pressure, are presented for these fundamental problems; for the jet impingement problems, surface properties such as pressure coefficients, shear stress, heat flux, and slip velocity are further provided as well. At the end, several DSMC simulations are performed and they validate the exact solutions.

These solutions are complex, involving both geometry and speed velocity ratio, S_0; they can supercede some current models, including the cosine law/Simons plume model. These solutions are the counterpart solutions to the continuum gaseous jet and jet impingement problems and, as a result, they reveal some new insights to these fundamental problems, and we may find many potential applications.

Acknowledgment

The authors gratefully acknowledge partial funding support from grants NSF-CBET-0854411, and NSF-DMS-0914706.

References

[1] Campargue, R., "Historical Account and Branching to Rarefied Gas Dynamics of Atomic and Molecular Beams: A Continuing and Fascinating Odyssey Commemorated by Nobel Prizes Awarded to 23 Laureates in Physics & Chemistry," *RGD24 International Symposium on Rarefied Gas Dynamics*, July 2004, pp. 32–64.

[2] Sanna, G., and Tomassetti, G., *Introduction to Molecular Beams Gas Dynamics*, Imperial College Press, London, 2005.

[3] Maev, R., and Leshchynsky, V., *Introduction to Low Pressure Gas Dynamic Spray*, Wiley-VCH, Weinheim, Germany, 2008.

[4] Hastings, D., and Garrett, H., *Spacecraft-Environment Interactions*, Cambridge Univ. Press, Cambridge, England, U.K., 1996.

[5] Sutton, G. P., and Biblarz, O., *Rocket Propulsion Elements*, 8th ed., John Wiley & Sons, Hoboken, NJ, 2010.

[6] Metzger, P., "Rocket Exhaust Cratering: a Serious Challenge for Space Exploration," *Proceedings of the 1st Workshop on Granular Materials in Lunar and Martian Exploration*, KSC, FL, Feb. 2005.

[7] Rebrov, A. K., "Free Jets in Vacuum Technologies," *Journal of Vacuum & Science Technologies (A)*, Vol. 19, No. 4, July–Aug. 2001, pp. 1679–1687.
doi:10.1116/1.1382649

[8] LeBeau, G. J., and Lumpkin, F. E., "Application Highlights of the DSMC Analysis Code (DAC) Software for Simulating Rarefied Flows," *Computer Methods in Applied Mechanics and Engineering*, Vol. 191, Nos. 6–7, Dec. 2001, pp. 595–609.

Downloaded by TEXAS A & M UNIVERSITY on March 20, 2013 | http://arc.aiaa.org | DOI: 10.2514/1.J051785

doi:10.1016/S0045-7825(01)00304-8
[9] Kannenberg, K. C., and Boyd, I. D., "Three-Dimensional Monte Carlo Simulation of Plume Impingement," *Journal of Thermophysics and Heat Transfer*, Vol. 13, No. 2, April–June 1999, pp. 226–235. doi:10.2514/z.6440
[10] Dietrich, S., and Boyd, I. D., "Scalar and Parallel Optimized Implementation of the Direct Simulation Monte Carlo Method," *Journal of Computational Physics*, Vol. 126, No. 4, 1996, p. 328–342. doi:10.1006/jcph.1996.0141
[11] Simons, G. A., "Effects of Nozzle Boundary Layers on Rocket Exhaust Plumes," *AIAA Journal*, Vol. 10, No. 11, 1972, pp. 1534–1535. doi:10.2514/3.6656
[12] Vashchenov, P., Kudryavstev, A., Khotyanovsky, D., and Ivanov, M., "DSMC and Navier–Stokes Study of Backflow for Nozzle Plumes Expanding into Vacuum," *RGD24 International Symposium on Rarefied Gas Dynamics*, Vol. 762, AIP Conference Proceedings, Monopoli, Italy, July 2004, pp. 355–360.
[13] Bartel, T. J., Plimpton, S., and Gallis, M. A., "Icarus: A 2-D Direct Simulation Monte Carlo (DSMC) Code for Multi-Processor Computers," User's Mannual-v.10.0., Sandian National Lab., Sandia Rept. SAND2001-2901, Albuquerque, NM, Oct. 2001.
[14] Bird, G. A., *Molecular Gas Dynamics and the Direct Simulation of Gas Flows*, Oxford Univ. Press, New York, 1994.
[15] Vincenti, W. G., and Kruger, Jr., Charles, H., *Introduction to Physical Gas Dynamics*, Krieger Publ., Malabar, Florida, 1986.
[16] Gombosi, T. I., *Gaskinetic Theory*, Cambridge Univ. Press, New York, 1994.
[17] Naumann, K. W., "The Freezing of Flow Deflection in Prandtl-Meyer Expansion to Vacuum," *RGD15 International Symposium on Rarefied Gas Dynamics*, Vol. 2, Grado, Italy, June 1988, pp. 524–533.
[18] Naumann, K. W., "Analytical Method for Rapid Estimation of Plumes from Small Satellite, Attitude Control Thrusters," *Rarefied Gas Dynamics: Proceedings of the 17th International Symposium*, Aachen, Germany, July 8–14, 1990 (A92-52701 22-77), VCH-Verlagsgesellschaft mbH, Weinheim, Germany, and New York, 1991, pp. 971–978.
[19] Noller, H. G., "Approximate Calculation of Expansion of Gas from Nozzles into High Vacuum," *Journal of Vacuum Science and Technology*, Vol. 3, No. 4, July 1966, pp. 202–207. doi:10.1116/1.1492475
[20] Narasimha, R., "Collisionless Expansion of Gases into Vacuum," *Journal of Fluid Mechanics*, Vol. 12, No. 3, 1962, pp. 294–308. doi:10.1017/S0022112062000208
[21] Woronowicz, M. S., "On Jet Flowfield Analysis and Simulation Techniques," AIAA Paper 1994-2048, June 2004.
[22] Dettleef, G., "Plume Flow and Plume Impingement in Space Technology," *Progress in Aerospace Sciences*, Vol. 28, 1991, pp. 1–71. doi:10.1016/0376-0421(91)90008-R
[23] Cai, C., "Theoretical and Numerical Studies of Plume Flows in Vacuum Chambers," Ph.D. Dissertation, Dept. of Aerospace Engineering, Univ. of Michigan, Ann Arbor, MI, 2005.
[24] Cai, C., and Boyd, I. D., "Theoretical and Numerical Study of Several Free Molecular Flow Problems," *Journal of Spacecraft and Rockets*, Vol. 44, No. 3, May–June 2007, pp. 619–624. doi:10.2514/1.25893
[25] Cai, C., and Boyd, I. D., "Collisionless Gas Flow Expanding into Vacuum," *Journal of Spacecraft and Rockets*, Vol. 44, No. 6, Nov.–Dec. 2007, pp. 1326–1330. doi:10.2514/1.32173
[26] Khasawneh, K., Liu, H., and Cai, C., "Surface Properties for Rarefied Circular Jet Impingement on a Flat Plate," *Physics of Fluids*, Vol. 23, No. 1, 2011, pp. 1–6. doi:10.1063/1.3549934
[27] Cai, C., and Wang, L., "Numerical Validations for A Set of Complete Gaskinetic Rocket Plume Solutions," *Journal of Spacecraft and Rockets*, Vol. 41, No. 1, 2011, pp. 59–69. doi:10.2514/1.A32046
[28] Liu, H., Cai, C., and Zou, C., "An Object-Oriented Implementation of The DSMC Method," *Computer and Fluids*, Vol. 57, No. 1, 2012, pp. 65–75. doi: 10.1016/j.compfluid.2011.12.007
[29] Chen, X., "The Impact Force Acting on a Flat Plate Exposed Normally to a Rarefied Plasma Plume Issuing from an Annular or Circular Nozzle," *Journal of Physics D: Applied Physics*, Vol. 43, No. 1, p. 315205. doi:10.1088/0022-3727/43/31/315205

S. Fu
Associate Editor

Downloaded by TEXAS A & M UNIVERSITY on March 20, 2013 | http://arc.aiaa.org | DOI: 10.2514/1.J051785